J Neurophysiol 99: 1020–1031, 2008.
First published November 28, 2007; doi:10.1152/jn.00942.2007.

Measurement and Analysis of Postsynaptic Potentials Using a Novel Voltage-Deconvolution Method

Magnus J. E. Richardson[1] and Gilad Silberberg[2]

[1]*Warwick Systems Biology Centre, University of Warwick, Coventry, United Kingdom; and* [2]*Department of Neuroscience, Nobel Institute for Neurophysiology, Karolinska Institute, Stockholm, Sweden*

Submitted 21 August 2007; accepted in final form 24 November 2007

Richardson MJ, Silberberg G. Measurement and analysis of postsynaptic potentials using a novel voltage-deconvolution method. *J Neurophysiol* 99: 1020–1031, 2008. First published November 28, 2007; doi:10.1152/jn.00942.2007. Accurate measurement of postsynaptic potential amplitudes is a central requirement for the quantification of synaptic strength, dynamics of short-term and long-term plasticity, and vesicle-release statistics. However, the intracellular voltage is a filtered version of the underlying synaptic signal and so a method of accounting for the distortion caused by overlapping postsynaptic potentials must be used. Here a voltage-deconvolution technique is demonstrated that defilters the entire voltage trace to reveal an underlying signal of well-separated synaptic events. These isolated events can be cropped out and reconvolved to yield a set of isolated postsynaptic potentials from which voltage amplitudes may be measured directly—greatly simplifying this common task. The method also has the significant advantage of providing a higher temporal resolution of the dynamics of the underlying synaptic signal. The versatility of the method is demonstrated by a variety of experimental examples, including excitatory and inhibitory connections to neurons with passive membranes and those with activated voltage-gated currents. The deconvolved current-clamp voltage has many features in common with voltage-clamp current measurements. These similarities are analyzed using cable theory and a multicompartment cell reconstruction, as well as direct comparison to voltage-clamp experiments.

INTRODUCTION

The extraction of synaptic amplitudes and waveforms from intracellular voltage traces is a basic component of electrophysiological analysis. However, the measurement of postsynaptic potential (PSP) amplitudes is complicated by the intrinsic filtering properties of the membrane: PSPs that are separated by timescales of the order of the membrane time constant overlap, leading to a distortion of the ongoing synaptic events. This is a common scenario for the types of presynaptic firing patterns used to probe the timescales of synaptic dynamics (Abbott et al. 1997; Thomson and Deuchars 1994; Tsodyks and Markram 1997). Many different methods have been used to account for preceding pulses, such as the fitting of an exponential decay and subtraction of the preceding pulses or the fitting of templates of averaged PSP shapes. These methods do not reveal the dynamics of the underlying signal and can become prohibitively laborious for voltage traces with large numbers of overlapping PSPs.

Here it will be demonstrated that an elementary deconvolution method can be used to significantly reduce the filtering of the synaptic drive in intracellular voltage traces measured away from the synapse and can be conveniently applied to the entire voltage trace in one step. The aim of the method is not to obtain the full dendritic filter, but rather to provide a simple procedure for the analysis and quantification of closely spaced PSPs. The method is applicable to cases of high variability and to nonpassive membrane dynamics such as the sag-rebound characteristic of the presence of the I_h voltage-activated current. The approach also reveals the synaptic signal at considerably higher temporal detail, allowing for the resolution of apparently unitary PSPs into component release events.

Deconvolution methods have a long history in signal analysis and have been introduced into the neurosciences on a number of occasions: in the analysis of synaptic amplitude histograms (Jack et al. 1981; Wong and Redman 1980; for a review see Dityatev et al. 2003), in the analysis of postsynaptic currents measured in voltage-clamp mode (Dempster 1986; for a review see also Neher and Sakaba 2003) to the inference of the somatic current from the spike rate of neurons with adaptation (Ahmed et al. 1998), and in the analysis of fast changes in functional MRI data (Hinrichs et al. 2000).

The principal effect of deconvolution on a signal is to sharpen it in time, by reversing the smoothing effect of some biophysical filtering process. In the context of intracellular voltage traces, it is the combined capacitive and conductive effects of the cell membrane that filter the synaptic drive (Rall 1967).

Here we demonstrate the considerable advantage of using this simple technique to measure the amplitudes and dynamics of synaptic events. The method, illustrated using both basic neuron models and multicompartment reconstructions, will be applied to a broad variety of experimentally measured connections. Although a biological interpretation of voltage deconvolution can be found, the deconvolution approach is a basic application of linear filter theory and as such does not strictly require a biological interpretation for its successful application (resolving closely spaced events). However, it will be seen that the underlying deconvolved signal shares many features of voltage-clamp current measurements, such as synaptic events with α-amino-3-hydroxy-5-methyl-4-isoxazolepropionic acid (AMPA) and γ-aminobutyric acid type A ($GABA_A$) kinetics clearly visible. The similarities and differences between the deconvolved voltage and voltage-clamp current will be examined in the DISCUSSION.

Address for reprint requests and other correspondence: M.J.E. Richardson, Warwick Systems Biology Centre, University of Warwick, Coventry CV4 7AL, United Kingdom (E-mail: magnus.richardson@warwick.ac.uk).

The costs of publication of this article were defrayed in part by the payment of page charges. The article must therefore be hereby marked "*advertisement*" in accordance with 18 U.S.C. Section 1734 solely to indicate this fact.

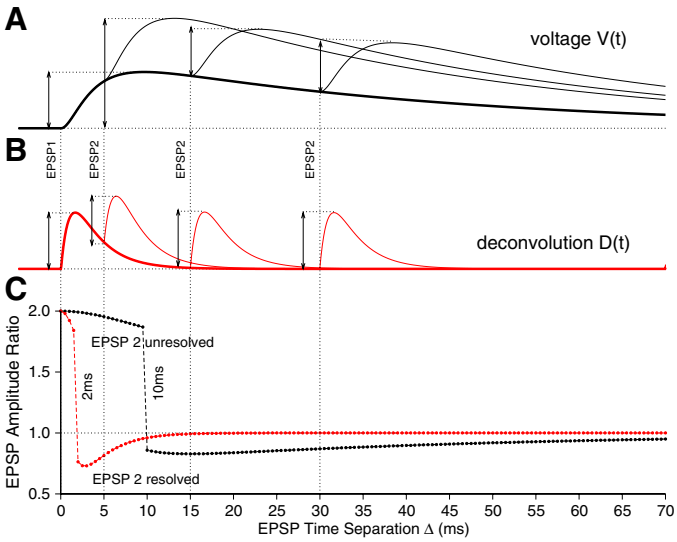

FIG. 1. Modeling the voltage deconvolution of a pair of excitatory postsynaptic potentials (EPSPs). Two EPSPs (3-ms rise time and 40-ms decay time; see METHODS) of identical strength arrive with onsets separated by a time Δ. *A*: example voltage traces for $\Delta = 5$, 15, and 30 ms. For $\Delta = 5$ ms the 2 EPSPs cannot be resolved because there is no intervening minimum. For $\Delta = 15$ and 30 ms the second pulses are diminished by the decay of the initial pulse. *B*: voltage deconvolution using a time constant $\tau = 40$ ms showing clear separation of all 3 pulse pairs. *C*: the ratio of the second EPSP amplitude to its true value, as measured from the voltage (black) and deconvolution (red) over a range of separations Δ. Resolution of the 2 pulses becomes possible for the voltage trace at $\Delta \simeq 10$ ms, whereas for the deconvolved trace they are resolvable already at $\Delta \simeq 2$ ms. For the purposes of illustration a naïve amplitude measurement method (minimum to maximum) has been used for this figure only.

METHODS

Experiments

Synaptic connections were recorded between neurons in rat somatosensory cortical slices, by using simultaneous whole cell patch recordings. The presynaptic cell was induced to produce a train of spikes separated by 50 ms, and the postsynaptic voltage (in current-clamp mode) or postsynaptic current (in voltage-clamp mode) averaged over ≥30 repeated sweeps. The cell pairs presented here are composed of layer 5 pyramidal-to-pyramidal and Martinotti cell-to-pyramidal connections measured in current-clamp mode, and pyramidal-to-pyramidal and pyramidal-to-basket cell connections measured in both voltage-clamp and current-clamp modes. Further experimental details are provided in Silberberg et al. (2004).

EPSP pair model

For the model neuron receiving two closely spaced excitatory postsynaptic potentials (EPSPs; used for Fig. 1) each EPSP $\mathscr{E}(t - t_0)$, with onset at time t_0, was modeled as a sum of three exponentials of amplitude a_k and time constant τ_k

$$\mathscr{E}(t - t_0) = \theta(t - t_0) \sum_{k=1}^{3} a_k \exp[-(t - t_0)/\tau_k] \qquad (1)$$

where $\theta(t - t_0)$ is the Heaviside, or step, function taking the value 0 for $t < t_0$ and 1, otherwise. The constants are $a = \{0.636, -2.01, 1.34\}$ mV and $\tau = \{1, 3, 40\}$ ms. The postsynaptic voltage trace is given by $V(t) = \mathscr{E}(t) + \mathscr{E}(t - \Delta)$, where Δ is the interval between the EPSP onsets in milliseconds.

Least-squares template-fit method

This method of extracting PSP amplitudes (Richardson et al. 2005a) provides a comparison (in Fig. 3*D*) for the deconvolution method. The voltage response $V(t)$ is matched, using a least-squares method, to a linear model with n_p PSP templates $\mathscr{E}_{\text{fit}}(t)$

$$V_{\text{fit}}(t) = \sum_{k=1}^{n_p} b_k \mathscr{E}_{\text{fit}}(t - t_k) \qquad (2)$$

For this method, each of the PSP templates is identical in form and built out of the difference of two exponentials

$$\mathscr{E}_{\text{fit}}(t) = \frac{\exp(-t/\tau_d) - \exp(-t/\tau_r)}{(\tau_r/\tau_d)^{\tau_r/(\tau_d - \tau_r)} - (\tau_r/\tau_d)^{\tau_d/(\tau_d - \tau_r)}} \qquad (3)$$

with the rise time constant τ_r, decay time constant τ_d, and amplitudes b_1, b_2, b_3, and so forth providing the free parameters of the fit. These parameters are varied until the difference between the fit voltage V_{fit} and the true voltage is minimized, in the least-squares sense.

Pyramidal cell model

The reconstructed layer 5 pyramidal cell shown in Fig. 6 (rat somatosensory cortex, PN day 15; see also Silberberg and Markram 2007) composed of 102 dendritic compartments and a soma. Its passive electrophysiological properties (capacitance $C_m = 1\ \mu\text{F}\cdot\text{cm}^{-2}$, conductance $g_m = 1/40{,}000\ \text{S}\cdot\text{cm}^{-2}$, giving $\tau_m = 40$ ms, resting voltage $E_m = -65$ mV, and axial resistance $R_a = 155\ \Omega\cdot\text{cm}$) were simulated using the software package NEURON (http://neuron.duke.edu; M. Hines, Yale University, New Haven, CT) with each compartment consisting of 50 segments. Six excitatory alpha synapses (reversal $E_s = 0$ mV, $\tau_s = 1$ ms, $g_s = 0.0002\ \mu$S) were placed on the dendritic structure at different distances from the soma. They were activated independently and both the somatic voltage in current-clamp mode and the current in voltage-clamp mode were measured in separate simulations. The somatic voltage clamp was implemented using the SEC1amp command with a target voltage of −65 mV and an access resistance $r_s = 0.1\ \text{M}\Omega$.

Deconvolution and reconvolution

The temporal derivatives used in the passive-membrane deconvolution $\tau\dot{x} + x = f$ are defined at time step $k = t/\text{d}t$ for time t, where dt is the time unit for each step, as $\tau(x_{k+1} - x_k)/\text{d}t + x_k = f_k$ to be consistent with the reconvolution x of a signal $f(t)$, which can be found through integration using the forward scheme $x_{k+1} = x_k + \text{d}t(f_k - x_k)/\tau$.

RESULTS

The effect of voltage deconvolution will first be illustrated by a simple model neuron receiving two closely spaced EPSPs. This model provides a basic motivation for the deconvolution method at a level of detail sufficient for its practical application (a more detailed cable-theory justification can be found in the APPENDIX). The method will then be demonstrated on a number of experimental examples that cover excitatory and inhibitory connections, as well as passive and nonpassive membrane responses.

Model: effect of deconvolution

An electrotonically compact model neuron is considered, with membrane properties characterized by a time constant τ

and resting potential E_m. The neuron receives a synaptic drive I_{syn} and so the voltage $V(t)$ at time t obeys the equation

$$\tau \frac{dV}{dt} = E_m - V + RI_{syn} \quad (4)$$

where R is the input resistance. The voltage solution to this equation would take the form of the synaptic current exponentially filtered over a timescale τ. In the context of experimental voltage recordings this filtering hinders experimental access to the fine temporal detail of synaptic events. However, a simple rearrangement of *Eq. 4* yields

$$E_m + RI_{syn} = \tau \frac{dV}{dt} + V \quad (5)$$

The left-hand side of this equation contains the unfiltered synaptic current and is identical to the defiltering of the voltage or, equivalently, the voltage deconvolution

$$D(t) = E_m + RI_{syn} \quad (6)$$

This deconvolution can easily be extracted from intracellular voltage traces by using the right-hand side of *Eq. 5*. All that is required is knowledge of the filter constant; the measured voltage is simply differentiated, multiplied by τ, and then added back to itself.

To interpret this process correctly, it is important to note that this defiltering is the removal of the principal filter (longest time constant) present in the recorded intracellular trace. It is not a measure of the full dendritic filter between the point of recording to the synapse itself. However, as will be seen, so long as this defiltering increases temporal resolution and can be reversed, it has a great deal of utility in the measurement of closely spaced PSPs. Further comment on the full dendritic filtering can be found in the DISCUSSION and APPENDIX.

This process is modeled in Fig. 1 using a protocol in which two EPSPs of identical synaptic strength are separated by a time Δ. The aim is to see when, in the voltage EPSPs or deconvolution pulses, the second event is discernible, and to measure its relative amplitude. In this modeled connection the EPSP rise time is 3 ms and the decay (or filter) constant is 40 ms. Superimposed voltage traces for this protocol are plotted in Fig. 1*A* for three pulse spacings: $\Delta = 5$, 15, and 30 ms. For the 5-ms spacing the two EPSPs are not resolvable as separate events, but appear as a single EPSP with twice the amplitude. For longer delays the second EPSP is resolved, but its amplitude (plotted as a function of Δ in Fig. 1*C*) is underestimated because it rides on the decay of the preceding EPSP. It can also be seen in this panel that the threshold for resolving the EPSPs into two separate events is at $\Delta = 10$ ms. Figure 1*B* shows the deconvolutions, using *Eq. 5*, corresponding to these three voltage traces. The deconvolution pulses are sharper because they decay with the EPSP rise time of 3 ms, and so the deconvolved EPSPs with $\Delta = 5$ are already resolved into two separate pulses, the threshold for this resolution being $\Delta \simeq 2$ ms. Thus closely spaced PSPs measured from the voltage trace can be accurately resolved only for spacings at a scale greater than the *decay time* of the EPSP—the membrane filter constant. However, the amplitudes measured from the deconvolved voltage are accurate at a much finer length scale—at a scale set by the *rise time* of the EPSP. Therefore the finer temporal resolution of the deconvolved traces allows for the composite structure of apparently unitary EPSPs to be easily distinguished (an experimental example of this is given later in Fig. 4).

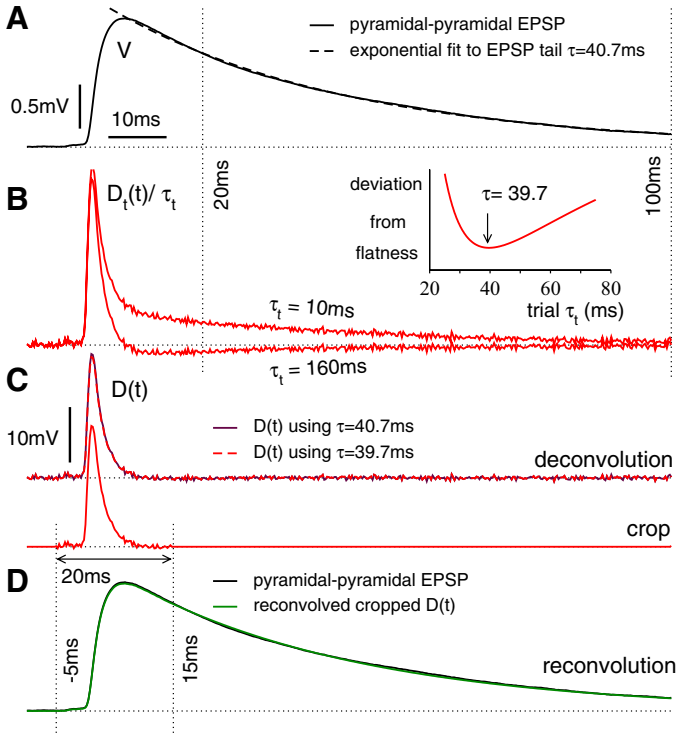

FIG. 2. Experimental measurement of the filter constant. *A*: an EPSP with exponential fit to the tail (20–100 ms after onset) yielding $\tau = 40.7$ ms. *B*: 2 deconvolutions (see *Eq. 7*) showing the effects of a trial filter constant that is 4× too small (10 ms) and above the baseline, or 4× too large (160 ms) and below the baseline. The *inset* is a measure of the deconvolution flatness (*Eq. 8*) over a region 20–100 ms after onset, when the trial time constant τ_t is varied. The minimum (nonzero due to the noise) occurs when $\tau_t = 39.7$ ms. *C*, *top superimposed traces*: the almost-identical deconvolutions for $\tau_t = 40.7$ and 39.7 ms. *Bottom trace*: the 20-ms-long cropped deconvolution with the noisy background replaced by the mean baseline. *D*: close agreement between the reconvolution of the cropped trace and the original voltage trace.

Experiment: a single EPSP

To perform the voltage deconvolution it is necessary to know the filter constant τ, which appears in *Eq. 5*. A direct approach would be to fit an exponential to the tail of an EPSP. Using the postonset period 20 to 100 ms (marked with dashed lines across Fig. 2*A*) this yields a decay time constant of $\tau = 40.7$ ms. However, for closely spaced EPSPs, this method is not always practicable. A second, *variational* method for finding τ will now be described.

MEASURING THE FILTER CONSTANT. A robust variational method, which can be easily extended to nonpassive voltage dynamics, may be derived from the fact that when a deconvolution is performed with the correct membrane filter constant the resultant trace $D(t)$ is flat away from the synaptic pulses (see Fig. 1). This is because in these intervening periods the neuron receives no synaptic input. In Fig. 2*B* two examples are given of a trial deconvolution $D_t(t)$ for which the chosen value of the filter constant τ_t is incorrect. It can be seen for this

excitatory connection that when τ_t is too small the deconvolution is above the baseline and if τ_t is too large the deconvolution is below the baseline. This is exactly what the simple model in *Eq. 4* predicts. If a deconvolution $D_t(t)$ is calculated with a trial decay constant τ_t it is straightforward to show that

$$D_t = \tau_t \frac{dV}{dt} + V = \frac{\tau_t}{\tau} D + \frac{(\tau - \tau_t)}{\tau} V \quad (7)$$

Thus a trial deconvolution with an incorrect time constant comprises a component of the true deconvolution $D(t)$ multiplied by a factor τ_t/τ and an erroneous second component proportional to the voltage. This second component introduces a long tail into the trial deconvolution and the prefactor $(\tau - \tau_t)$ determines whether the erroneous contribution is above or below the baseline. Clearly, when $\tau_t = \tau$ the prefactor is zero, the voltage contribution vanishes, and the resultant quantity (*Eq. 7*) becomes equivalent to the true deconvolution D given by *Eq. 5*.

This feature may be used to find the correct τ by examining the trial deconvolution for flatness over some region t_1 and t_2 after the onset as τ_t is varied. This region should be chosen so that the EPSP has fully risen and only the decaying component remains. A measure of the flatness that yields robust results is the mean square of the trial deconvolution (*Eq. 7*) normalized by τ_t

$$\frac{1}{(t_2 - t_1)} \int_{t_1}^{t_2} ds \left(\frac{dv}{dt} + \frac{v}{\tau_t} \right)^2 \quad (8)$$

where $v = V - E_m$ is the voltage relative to the baseline resting potential E_m. Normalization by τ_t is necessary so that the effect of noise (the overwhelming majority of which comes from the differential term of *Eq. 7*) is treated equally as τ_t is varied. In the *inset* of Fig. 2*B* the flatness measure in *Eq. 8*, with $t_1 = 20$ ms and $t_2 = 100$ ms after the EPSP onset, is plotted for different τ_t. The value that gives the flattest trace is $\tau_t = 39.7$ ms. As expected, this result is consistent with the direct exponential measurement, which yielded 40.7 ms. The voltage deconvolutions with these two time constants are shown to be practically identical in Fig. 2*C*.

It should be noted that in the preceding, the filter time constant τ for the decay of the PSP was measured directly from the voltage trace itself. The filtering properties of cells, as encoded by the membrane time constant, can also be probed by injecting square-pulse currents into the soma. Simple point-neuron models, which neglect dendritic structure, suggest that the somatically measured membrane time constant and PSP decay constant are identical. However, this is not necessarily the case for neurons that have extended dendritic structures such as pyramidal cells; geometric effects (Agmon-Snir and Segev 1993) and nonuniform channel densities (London et al. 1999), particularly those located far from the soma, such as the h-current, make signal filtering from synapse to soma dependent on the synaptic location. Injecting square-pulse currents at the soma, however, probes only the membrane properties electronically local to the soma. For this reason the filter constant used for a specific synaptic connection is best measured from the voltage trace itself. This has the added advantage of making the deconvolution–reconvolution method self-contained in the sense that only the voltage trace itself is required.

CROP AND RECONVOLUTION. The short deconvolved pulse seen in Fig. 2*C* decays quickly, with the rise constant of the original EPSP. It may be cropped out of the trace, in this case 5 ms before and 15 ms after the pulse onset, by replacing the noisy baseline outside this region with its average value, and then reconvolved using the integral solution for V of *Eq. 4*

$$V_c(t) = \int_0^t \frac{ds}{\tau} e^{-(t-s)/\tau} D_c(s) \quad (9)$$

where D_c is the cropped deconvolution. The algorithm for calculating this integral from data is provided in METHODS. This *reconvolved* voltage is compared with the true voltage in Fig. 2*D* and seen to be in close agreement, demonstrating that almost all the information required to reconstruct the EPSP is contained in the decay constant and the underlying deconvolved pulse. This deconvolution–reconvolution exercise is unremarkable for a single EPSP, but as will now be shown, it can be used to isolate closely spaced EPSPs.

Experiment: separating trains of PSPs

The deconvolution–crop–reconvolution method is now applied to a typical experimental paradigm used for measuring synaptic dynamics: an averaged voltage trace consisting of eight EPSPs separated by 50 ms (Fig. 3*A*). The same pair of cells from Fig. 2 was used so the filter constant is again 40 ms (Fig. 3*A*, *inset*). However, this quantity could equally well be found from a flatness criterion, where for this case regions around all of the pulses would need to be masked out.

The voltage response and its deconvolution are plotted in Fig. 3*A*. It can be seen that the deconvolution $D(t)$ is resolved into a well-spaced train of pulses, where the flat regions between each pulse signify that the filter constant was correctly estimated and, furthermore, that the assumption of a linear summation of PSPs is a good one, despite the large amplitude of this connection. In Fig. 3*B* the deconvolved pulses are shown in detail. Their superposition (Fig. 3*B*, *inset*) demonstrates that they retain the same shape despite the vesicle rundown in this synapse, which exhibits synaptic depression (Abbott et al. 1997; Tsodyks and Markram 1997). The relative baseline-to-peak amplitudes are plotted in Fig. 3*D*. It can be further noted that, although some residual filtering from the dendrites will still be present, the decay constants (2 ms) of the deconvolution pulses in Fig. 3*B* are consistent with that of AMPA kinetics.

The amplitudes of the separated EPSPs can be obtained by cropping and reconvolving the deconvolved pulses. The intermediate cropped traces are plotted in Fig. 3*C*. These can be reconvolved to yield the eight *isolated* EPSPs plotted in Fig. 3*C* (*bottom set* of green curves) and from which the absolute EPSP amplitudes can be easily read off (plotted in Fig. 3*D*). As a "checksum," the isolated EPSPs can be summed together and compared with the original voltage waveform. This comparison is also plotted in Fig. 3*C* above the isolated EPSPs where it can be seen that the agreement is such that it is difficult to discern the two traces. This checksum is an important step that provides verification of the method. If the resummed PSPs are

significantly different from the original voltage trace, it signals that there are membrane filtering effects present that are not captured correctly by the passive filter model given in *Eq. 4*. This might be due to the activation of voltage-gated currents. For such cases a more complex model must be used; this will be subsequently introduced in *Nonpassive membranes*.

In Fig. 3*D* a least-squares fit method (see METHODS) is compared with the measurement of the amplitudes (relative to the initial EPSP) from the deconvolved pulses and the reconvolved EPSPs. It can be seen that the three methods give closely similar results. However, care should be taken for cases where the successive deconvolved pulses have different shapes (this was not the case here, as shown in Fig. 3*B*, *inset*). If this is the case, then the pulses should be reconvolved and it is the amplitude of the reconvolved PSPs that must be used.

Experiment: fluctuating voltage traces

The deconvolution method can also be used to analyze traces with higher variability, such as a recording of spontaneous activity in vivo or a single sweep instead of the averaged EPSP trains that were used in Fig. 3. In Fig. 4 such a sweep is presented. Although the voltage is strongly fluctuating, the deconvolution procedure again produces a train of well-separated pulses. Its higher resolution allows fine detail, such as the double event in the second pulse, to be clearly resolved. This resolution of two closely spaced EPSPs (with separation $\Delta \simeq 5$ ms) provides an experimental example of the separation effect of deconvolution that was modeled in Fig. 1—a feature that has obvious application to the resolution of synaptic timing events. This resolution of apparently unitary events is analogous to that used for vesicle release-rate analysis in voltage-clamp current traces (Dempster 1986; Neher and Sakaba 2003), and so has the potential to facilitate greatly the measurement of vesicle-release statistics from voltage traces.

Nonpassive membranes

Many neurons show the effects of subthreshold voltage-gated channels, such as the h-current sag/rebound, in their response to synaptic input or current injection. The passive filter model of *Eqs. 4* and *5* is not general enough to capture the response properties of neurons that show the effects of activated voltage-gated currents. However, the model can be extended easily by considering a multivariable linear model of the voltage dynamics (Brunel et al. 2003; Cox and Griffith 2001; Hodgkin and Huxley 1952; Koch 1984; Koch and Segev 1998; Mauro et al. 1970; Richardson et al. 2003; Rinzel and Ermentrout 1989; Surkis et al. 1998) to deconvolve the voltage correctly in the presence of voltage-gated currents.

MODELING NONPASSIVE MEMBRANES. Here the passive model is generalized to two variables, consisting of the voltage v (mea-

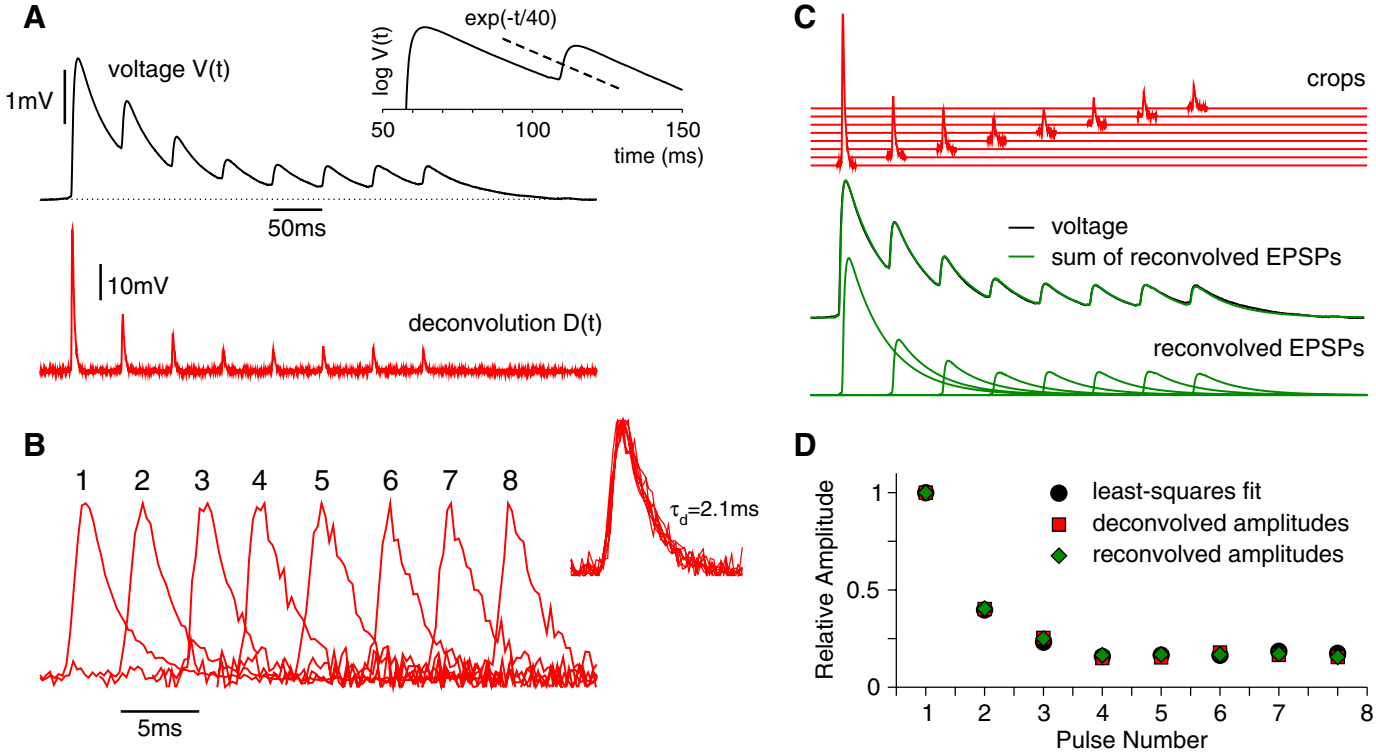

FIG. 3. The deconvolution method applied to a pyramidal-to-pyramidal connection exhibiting synaptic depression. *A*: the averaged postsynaptic voltage triggered by 8 presynaptic action potentials separated by 50 ms (black). The semilog plot *inset* shows the first 2 EPSPs together with an exponential decay of time constant 40 ms (dashed line). This decay constant is used to generate the deconvolution (red) using *Eq. 5*. *B*: an expanded view of the 8 deconvolved pulses with scaled amplitudes. Their superposition (*inset*) shows that the pulses are of similar shape, with a 2-ms decay constant consistent with α-amino-3-hydroxy-5-methyl-4-isoxazolepropionic acid (AMPA) kinetics. *C*: in red are the 8 cropped deconvolutions (−5 to 15 ms around each pulse). The separated EPSPs from the reconvolved cropped pulses are shown (*bottom plot*, green). Just above is the sum of these isolated EPSPs (also green), which is almost fully superimposed on the voltage trajectory (black). *D*: the relative amplitudes (as would be needed for the quantification of short-term synaptic plasticity) measured using 3 different methods; a direct least-squares fit to the trajectory (black circles), the amplitudes of the deconvolved pulses from *A* (red circles), and the amplitudes measured from the reconvolved pulses in *C* (green diamonds).

sured from the baseline $v = V - E_m$) and a second variable w. This variable affects the voltage with a strength γ, proportional to the excess current flowing through the voltage-gated channels, and itself follows the voltage with a time constant τ_w. The two equations describing the voltage v and membrane-current variable w can be written

$$\tau_v \frac{dv}{dt} = -v - \gamma w + D \quad (10)$$

$$\tau_w \frac{dw}{dt} = v - w \quad (11)$$

where $D(t)$ would again be proportional to the synaptic drive for a compact cell. The voltage-gated current variable w is hidden from direct experimental view; its behavior, governed by γ and τ_w, is inferred from the effect it has on the voltage. Its explicit appearance in the two equations can be made implicit by integrating *Eq. 11* between 0 and t [with the assumption that the neuron is at its resting voltage $v(0) = w(0) = 0$ at $t = 0$] to yield w in terms of v as

$$w(t) = \int_0^t \frac{ds}{\tau_w} e^{-(t-s)/\tau_w} v(s) \quad (12)$$

which can then be inserted into *Eq. 10* to yield an equation for the voltage only. It is straightforward to rearrange this to give the deconvolved voltage $D(t)$ (analogous to *Eqs. 5* and *6*) at time t

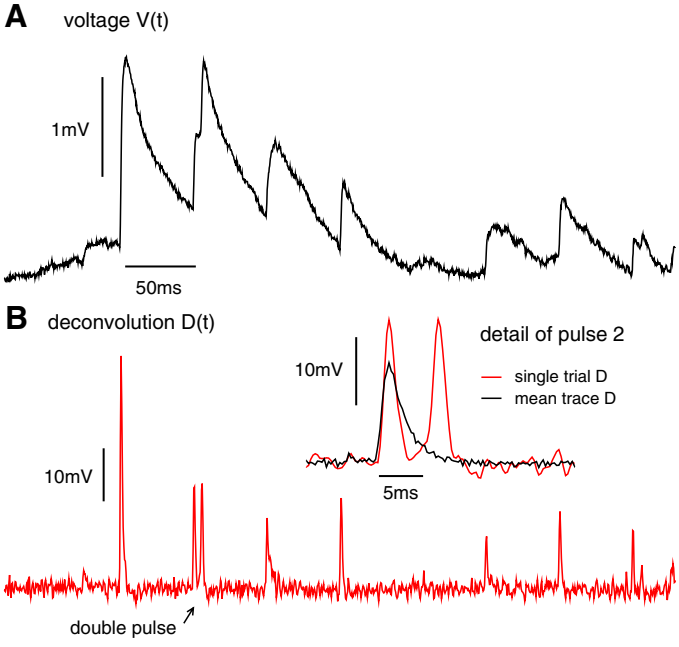

FIG. 4. The deconvolution of an unaveraged voltage sweep. *A*: a single voltage sweep chosen from the data set that yielded the averaged voltage trace in Fig. 3*A*. *B*: its deconvolution using $\tau = 40$ ms. The pulses are now well separated with the second PSP clearly resolved into 2 closely spaced events. The *inset* compares an expanded view of the deconvolution of this double event with the deconvolution of the mean trace of Fig. 3*A*.

$$D = \tau_v \frac{dv}{dt} + v + \gamma \int_0^t \frac{ds}{\tau_w} e^{-(t-s)/\tau_w} v(s) \quad (13)$$

This is the two-variable extension of the passive deconvolution. The first two terms on the right-hand side of this equation are identical to the passive form (*Eq. 5*) with time constant τ_v, but the equation also comprises an additional term that accounts for the activation of the voltage-gated currents.

To perform a passive, one-variable deconvolution the only free parameter to be extracted from experiment is the membrane filter constant τ. However, *Eq. 13* requires three parameters: τ_v, τ_w, and γ. The variational approach coupled with a flatness criterion, as illustrated in Fig. 2 for passive cells, can be used to obtain these unknown quantities. The method is as follows: *1*) an initial set of parameters τ_v, τ_w, and γ is used to deconvolve the voltage trace using *Eq. 13*; *2*) the flatness of the trace is then examined away from the underlying pulses (the pulses are cut using some appropriately sized window around the identified onsets); *3*) this is repeated over a range of each of τ_v, τ_w, and γ until the flattest trace is found; and *4*) the crop and reconvolution stages are then carried out in the same way as was shown in Fig. 3, except that for the reconvolution it is the integration of *Eqs. 10* and *11* that is required.

It can be noted that, as a by-product of this procedure, the method provides all the parameters required to generate reduced models that treat active membranes in the linear approximation.

EXPERIMENT: NONPASSIVE MEMBRANES. In Fig. 5 two examples are given [trains of EPSPs and inhibitory postsynaptic potentials (IPSPs)] of the two-variable deconvolution method applied to cells with sag/rebound responses characteristic of the h-current (Silberberg and Markram 2007).

For Fig. 5, *A–C*, the case of an EPSP train, the deconvolved pulses have a decay constant of 2 ms, consistent with AMPA kinetics. Thus despite the very different membrane response, the two-variable deconvolution yields an underlying pulse that is very similar to that seen for the deconvolution of the cell with a passive voltage response in Fig. 3.

For the IPSP train in Fig. 5, *D–F* the deconvolved pulses show a 10-ms decay constant, consistent with $GABA_A$ kinetics. Although the summation of the reconvolutions agrees well with the original voltage trace, the deconvolved pulses are at the limit of what can be considered separated. This is because the $GABA_A$ decay constant is of an order similar to that of the pulse separation of 50 ms. A shorter separation would give rise to the effect demonstrated in Fig. 1, *B* and *C* for $\Delta < 15$ ms (that model was of an excitatory connection with AMPA-like kinetics) for which subsequent deconvolved pulses are affected by the decay of those preceding.

Before concluding this section, it should be noted that the two-variable method easily generalizes to more complex membrane responses that require three or more additional w variables. Such dynamics can be accounted for by adding extra interaction terms

$$\tau_v \frac{dv}{dt} = -v - \sum_n \gamma_n w_n + D \quad (14)$$

with n equations for w_n of the form of *Eq. 11*. In this way a

broad range of dynamics can be handled—equations of the linear form (*Eq. 14*) have already been used to model the effects of: sodium and potassium spike-generating currents near threshold (Hodgkin and Huxley 1952); calcium-activated potassium adaptation currents (Fuhrmann et al. 2002); and persistent-sodium and slow-potassium currents (Richardson et al. 2003). Finally, it should be noted that the parameters τ_v, γ, and so forth, which were found by a variational method here, have a clear biophysical interpretation and can be systematically related to the underlying conductance-based model of the neuron (Koch 1984).

DISCUSSION

A deconvolution technique was demonstrated that defilters voltage traces to leave a signal with higher temporal detail from which EPSPs may be readily extracted and their amplitudes measured. The generality of the method was established through a variety of experimental examples, including both AMPA and $GABA_A$ synapses and neurons with passive and nonpassive membranes.

As a final part of the analysis, two aspects of the method will be examined in more detail. First, the scope of the linearity assumption, which is shared by any technique that measures PSP amplitudes from intracellular voltage traces, will be assessed. Second, the similarity between the deconvolved voltage waveform and voltage-clamp current measurements will be investigated using cable theory and further experiments.

Strongly nonlinear voltage-gated currents

The deconvolution–reconvolution method requires that the filter properties remain constant throughout the recording, i.e., that τ for the passive case in *Eq. 5* or τ_v, γ, and τ_w for the two-variable case in *Eq. 13* do not change their values during the measurement process. Two cases of neurons showing the effects of voltage-gated currents were treated in Fig. 5 and from the checksum in Fig. 5, *C* and *F* it can be seen that the membrane response properties do remain constant over the period of the experiment, despite the fact that the connections were strong ones. However, it is possible that for considerably stronger activation or for different classes of voltage-gated currents with sharper activation curves, the linear approximation (Hodgkin and Huxley 1952; Koch 1984) underlying the two-variable deconvolution would not be as valid. Such nonlinearities would temporarily disrupt any method that attempts to measure synaptic amplitudes from the intracellular voltage. Deconvolution methods can be augmented to deal with nonlinearities, for example the nonlinear delayed glutamate clearance at the calyx of Held (Neher and Sakaba 2001), but

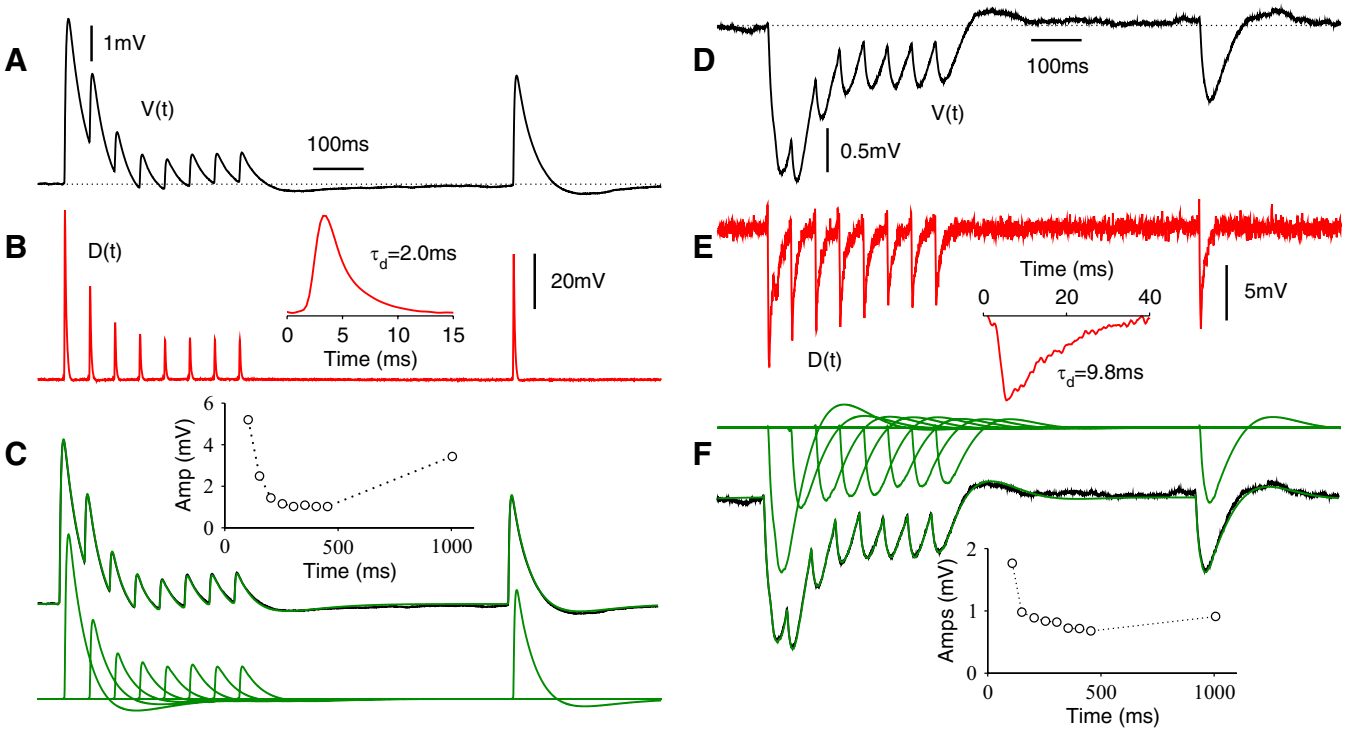

FIG. 5. Deconvolution for nonpassive voltage responses. *A–C*: pyramidal-to-pyramidal EPSPs. *D–F*: Martinotti-cell-to-pyramidal inhibitory postsynaptic potentials (IPSPs). *A*: averaged 8-pulse EPSP train, each separated by 50 ms, followed 550 ms later by a final EPSP. This connection exhibits a late below-baseline sag, typical of the h-current. *B*: a 2-variable deconvolution (*Eq. 13* with τ_v = 36 ms, γ = 0.8, and τ_w = 150 ms) removes the effects of the nonpassive membrane filtering to produce a set of well-separated pulses. The deconvolution parameters were found by applying a flatness criterion to the whole trajectory, with the exception of a window 4 ms before and 21 ms after each pulse. The *inset* shows the underlying average pulse has a 2-ms decay constant, consistent with AMPA kinetics. *C*: the crop and reconvolution procedure, using the same window described earlier, yields the isolated EPSPs (*bottom set* of green curves) from which the amplitudes may be measured (*inset*). The superimposed top pair of curves compares the sum of the isolated EPSPs (green) with the original *voltage trace* (black), showing good agreement. *D*: averaged voltage response of the pyramidal cell due to similar presynaptic stimulation of a Martinotti interneuron. An h-current response is seen in the IPSP tail. *E*: the deconvolution, using τ_v = 74 ms, γ = 1.6, and τ_w = 72 ms (this cell is different from that in *A–C*) with the flatness criterion applied to the whole trajectory, with the exception of a window 4 ms before and 41 ms after each pulse. The *inset* shows underlying pulses with a 10-ms decay constant, consistent with γ-aminobutyric acid type A kinetics. *F*: the superposition of the summed isolated IPSPs again agrees well with the original voltage trace.

nonlinear effects are considerably richer in their dynamics and must be dealt with on a case-by-case basis (i.e., requiring knowledge of the voltage dependence of the filter constant, as was seen in Supplemental Fig. 2 of Chadderton et al. 2004). In any such case, the linear deconvolution method presented here can be used to identify when such nonlinear effects are significant via the checksum procedure illustrated in Figs. 3*C* and 5, *C* and *F*.

Synaptic reversal potential nonlinearities

Synaptic current is voltage dependent and thus PSP amplitudes depend on the voltage at the location of the synapse. Because preceding PSPs bring the voltage closer to the synaptic reversal potential, this will reduce the current flowing through subsequent channel openings at the same synapse. It was recently noted (Banitt et al. 2005) that this can lead to a type of synaptic depression. For excitatory connections this effect is weak due to the large difference between the rest and AMPA synapse reversal potential (see Banitt et al. 2005, in which the extended shape of the neuron is accounted for; an example of an excitatory synapse is given in which this effect is estimated at 5%). However, for very strong EPSPs, and particularly IPSPs, the relation between the measured voltage amplitude and conductance amplitude will be nonlinear, and any method that extracts synaptic amplitudes from the somatic voltage traces will suffer from this problem. For neurons that are noncompact some estimation of the voltage at the synapse itself must be used to probe the synaptic waveform. This unavoidably requires the use of more sophisticated and involved methods such as the voltage-jump method introduced by Häusser and Roth (1997), simulations of multicompartment reconstructions of cells (Banitt et al. 2005), defiltering of voltage-clamp recordings for synapses with a measurable *N*-methyl-D-aspartate (NMDA) component (Kleppe and Robinson 1999), or, as has been proposed on theoretical grounds, a combination of multisite recordings (Cox 2004). Nevertheless, in two experimental comparisons (subsequently shown in Fig. 7) of amplitudes measured in voltage-clamp and current-clamp modes no synaptic nonlinearities are seen, suggesting that, at least for EPSPs, this effect is not significant.

Deconvolution and voltage-clamp current

The deconvolved waveforms, in which the AMPA or $GABA_A$ receptor kinetics can be seen in the pulse decays, show a striking similarity to the current measured in voltage-clamp mode. This similarity will now be examined through modeling and experiment, with the mathematics underlying the modeling to be found in the APPENDIX.

MODEL NEURON WITH TWO DENDRITES. A basic model is first considered with a soma of surface area A_s and two passive dendrites with space constant λ and radius a (see Fig. 6*A* and the APPENDIX for further details). One dendrite receives an instantaneous charge injection at time $t = 0$ either proximally $\lambda = 0.1$, or distally $\lambda = 0.5$. An example of the spatial voltage distribution is given for the current-clamp and voltage-clamp modes in Fig. 6*B* at three different times and for a case for which $A_s = A_d$, where A_d is an electrotonic length constant's worth of dendritic surface area. Cable theory (Tuckwell 1988) states that current flowing into the soma is proportional to the dendritic voltage gradient near the soma. The spatial voltage distributions for the current-clamp and voltage-clamp cases are different, and so the currents flowing from the activated dendrite into the soma are not the same.

Sharpness of the filtering. The synapse was modeled as being fast (delta-pulse) and so the spread of the deconvolution and voltage-clamp current waveforms at the soma directly give the filter shape. For voltage clamp, the current at the soma is independent of the somatic area; this is plotted in black for the distal and proximal synapses in Fig. 6*C*. The deconvolved somatic voltages (plotted with the sign inverted) are shown for proximal and distal synapses in the same panels for different ratios $\rho = A_d/A_s$ of the dendritic to somatic areas. In all cases the deconvolution waveform is sharper than that of the voltage-clamp current. This is particularly clear for distal synapses on a neuron with a relatively small soma (dot-dashed red line, Fig. 6*C*, *right*): for the case of a distal synapse on a dendrite of length $L = 0.5\lambda$ it can be shown that the voltage-clamp filter time constant is fourfold longer than that of the deconvolution filter (see the APPENDIX).

Large somata. If the synaptic area of the soma is large then the input resistance will be dominated by the somatic resistance. In this limit the soma does not significantly depolarize, and thus the deconvolution waveform (*Eq. 6*) is identical to the voltage-clamp current waveform. This effect can be seen in Fig. 6*C* when the model neuron has a dendritic–somatic area ratio of 0.25.

Proximal and distal synapses. When the synapse is close to the soma, the somatic voltage initially charges up but then, after a certain time (see APPENDIX), this charging becomes inferior to the current lost due to charge dissipation along the dendrite (see also Roth and Häusser 2001). At this point, the deconvolution filter changes sign, resulting in a weak overshoot, as is just visible in Fig. 6*C* (*left*, dot-dashed red line). This effect becomes increasingly negligible as the synapse becomes more distal. It should be further noted that both the voltage-deconvolution and voltage-clamp filters have shapes dependent on the synapse location.

In summary, voltage-clamp measures the current flowing into the soma when the somatic voltage is clamped, whereas deconvolution measures the net current into the soma when the neuron is in its natural current-clamp state, i.e., the difference between the magnitudes of the currents flowing into and out of the soma (see APPENDIX). For large somata, the soma does not depolarize significantly and so the deconvolution and voltage-clamp current waveforms become identical. In all cases the deconvolved waveform is sharper than the voltage-clamp current. These results are derived mathematically in the APPENDIX.

MULTICOMPARTMENTAL PYRAMIDAL-CELL MODEL. Results from the analyses of the simplified model also hold for a model with a more realistic dendritic structure: a layer 5 pyramidal-cell reconstruction (see Fig. 6*D*). A passive membrane has been chosen so that the spatial effects may be the focus of concentration. Synapses with identical time constants and peak conductances (see METHODS) were placed at various positions on the dendrites and the corresponding somatic EPSPs and excitatory postsynaptic currents recorded (see Fig. 6*E*), with synapse 1 the most proximal and 6 the most distal. In Fig. 6*F* the waveforms (normalized to the same peak) of the deconvolved voltage (red), voltage-clamp current (black), and synaptic cur-

rent (green) are compared for each of these contacts. For synapse 1, the most proximal, it is seen that the voltage-clamp current gives a good account of the synaptic current, whereas the deconvolution (plotted upside-down) has a weak overshoot (this is due to the change of sign in the tail of the filter discussed earlier). As the synapse is placed more distally, the overshoot becomes less significant and the deconvolution is seen to give a sharper picture of the synaptic current than the voltage-clamp current.

EXPERIMENTAL COMPARISON. Figure 7 shows the waveforms and amplitudes measured from voltage-clamp current and voltage deconvolution for two connections: a pyramidal-to-pyramidal connection, for which the postsynaptic cell is not electrotonically compact; and a pyramidal-to-basket cell connection, for which the postsynaptic cell is electronically more compact.

In reference to the synaptic nonlinearities discussed previously, it can be noted that for both connections the relative amplitudes measured from the two methods are seen to be in good agreement (Fig. 7, *D* and *I*) with no discernible effect of the synaptic reversal potential. For the pyramidal-to-pyramidal cell the weak systematic trend (the initial larger amplitudes are stronger for deconvolution than for voltage-clamp current) is actually the reverse of what would be expected for synaptic nonlinearities, and could potentially be due to a weak drift in parameters such as synaptic efficacy or ionic concentrations during the course of the experiment.

Figure 7*E* shows details of the pulse shape for the two methods (the deconvolution is again plotted upside-down for comparison) with the deconvolved waveform considerably sharper than the voltage-clamp current. This is what was predicted by the models in Fig. 6 for this class of electronically extended cell, for which a perfect space clamp is not possible.

In the pyramidal-to-basket cell connection the current-clamp voltage (Fig. 7*F*) comprises EPSPs with two decay components at 6.8 and 60 ms, the latter of which is not seen in response to somatic step-current injection for this interneuron class (Silberberg et al. 2004) but is present in the voltage-clamp current (Fig. 7*G*). Thus it is the faster 6.8-ms component that arises from the membrane filtering and is used for the deconvolution plotted in Fig. 7*H*. The shapes of the waveforms are compared in Fig. 7*J* (normalized to have the same peak outward current and aligned at the point of initiation). The component with the 60-ms time constant is stronger in the deconvolved waveform than that in the voltage-clamp current. Because in voltage-clamp mode the depolarization at the synapse is suppressed as compared with the natural state (current-clamp mode) of the neuron, this relative decrease in the strength of the longer component is consistent with its being depolarization activated and potentially an NMDA component to the synaptic current, although other mechanisms are not ruled out.

In summary, although the voltage-deconvolution and voltage-clamp current waveforms give rather close results for PSP

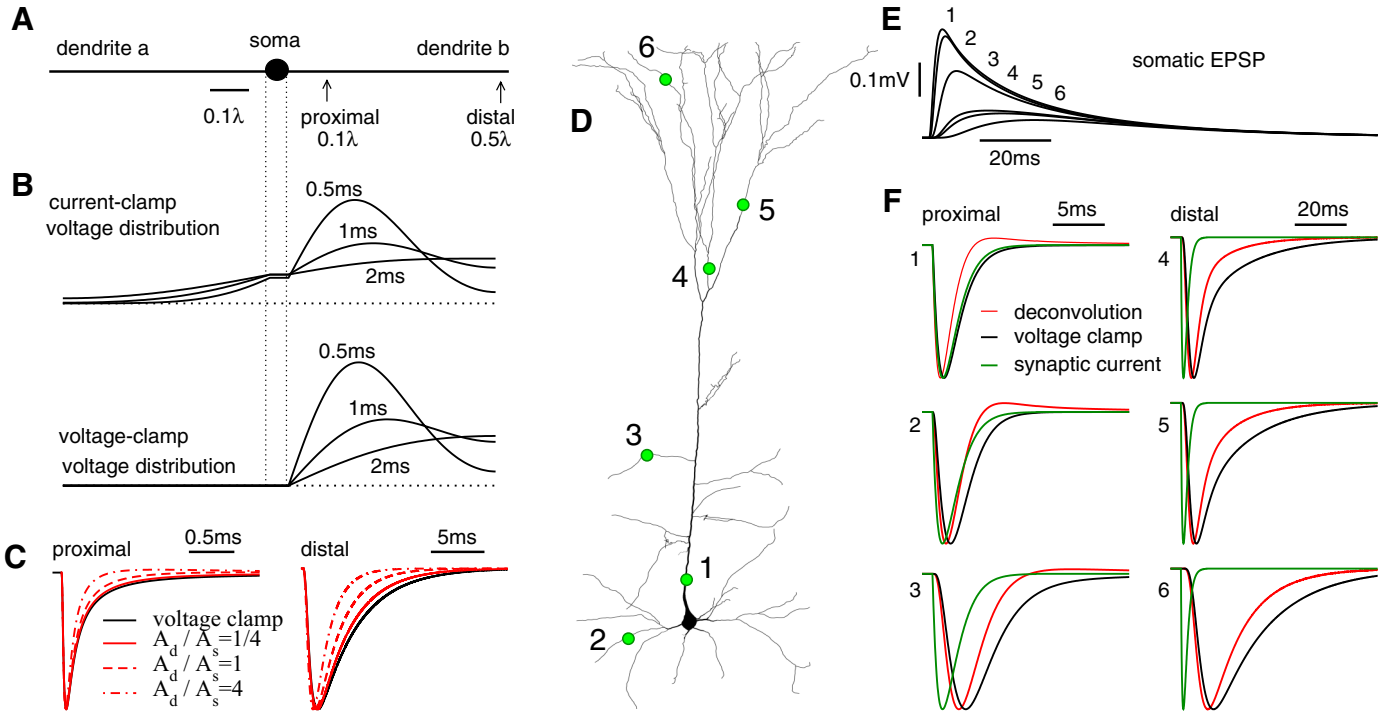

FIG. 6. Modeling the dendritic filtering for voltage-clamp current and voltage deconvolution. *A*: a simple model neuron with 2 dendrites, labeled *a* and *b*, each of length 0.5 space constants λ. The effects of instantaneous charge injection, either proximal 0.1λ or distal 0.5λ to the soma are considered for different ratios of the effective dendritic area to somatic area $\rho = A_d/A_s$. *B*: the spatial voltage distribution for current-clamp and voltage-clamp modes for a proximal charge injection with $\rho = 1$ displayed at 3 different times. *C*: a comparison of the deconvolved somatic voltage (*Eq. 6* with the sign inverted) and the voltage-clamp current for proximal and distal charge injection. The shape of the responses measured at the soma provide the filter profiles for the 2 clamp modes and are clearly dependent on the synapse location for both modes. In all cases the deconvolution filter is sharper than the voltage-clamp current. For the proximal case with small soma ($\rho = 4$, red dot-dashed line), a very weak overshoot after about 0.5 ms can be seen. For larger somata ($\rho = 0.25$) the deconvolved voltage (red solid line) and voltage-clamp current waveforms become identical. *D*: reconstructed layer 5 pyramidal cell with 6 synapses placed at various distances from the soma. *E*: somatic EPSPs for these synapses. *F*: normalized deconvolved EPSPs and voltage-clamp current waveforms. The response shows the same synaptic-position dependence as was demonstrated in the simplified model in *A–C*. For distal synapses the deconvolution waveform is sharper than the voltage-clamp current.

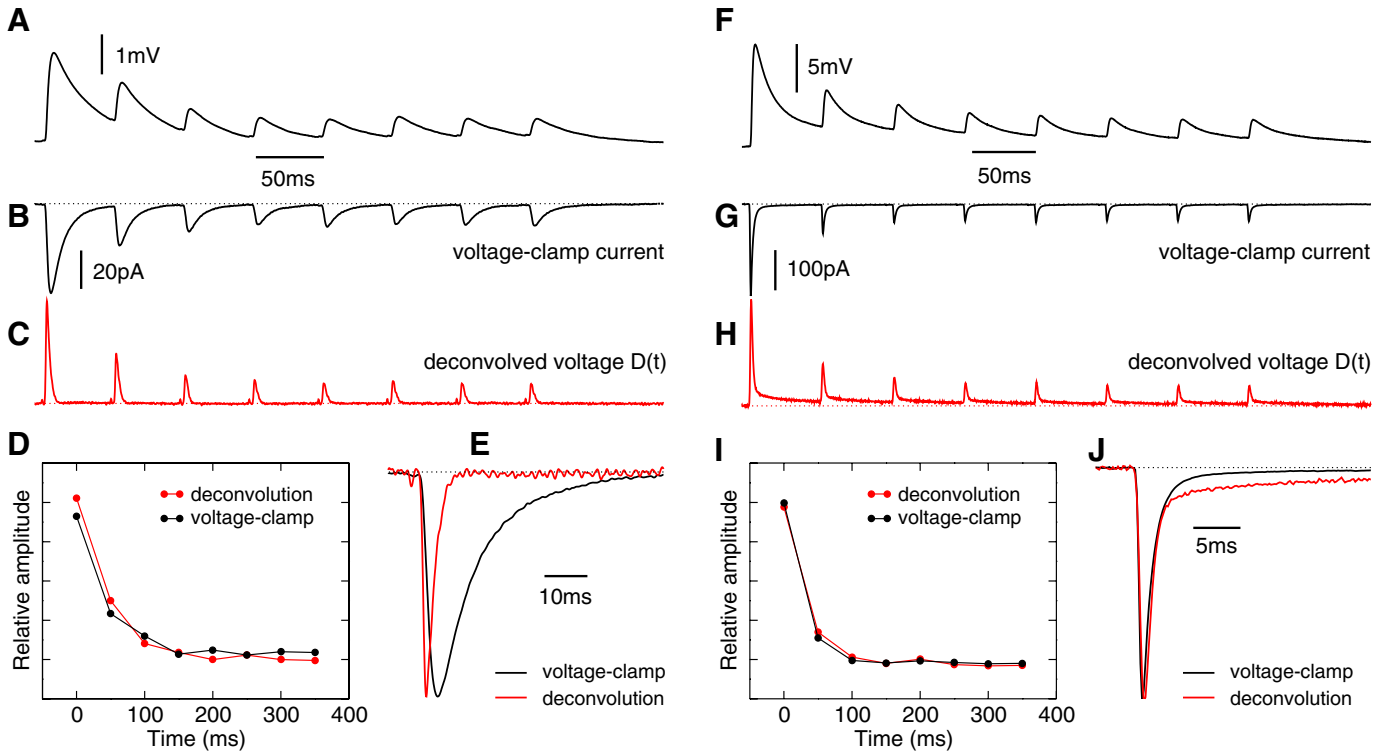

FIG. 7. Experimental comparison between voltage-clamp current and voltage deconvolution for 2 connections. *A–E*: pyramidal-to-pyramidal connection. *A*: averaged voltage measured in current-clamp mode showing EPSPs with decay constant 23 ms. *B*: averaged current measured in voltage-clamp mode. *C*: voltage deconvolution of the trace in *A*. *D*: comparison of the relative EPSP amplitudes (normalized by the average amplitude for each train) showing good agreement between the 2 methods. *E*: detail of the pulses: the deconvolved pulse (sign reversed) is considerably sharper, decaying with the AMPA kinetics of 1.9 ms, whereas the voltage-clamp current (decay 11 ms) shows the effect of the partial space clamp for this electrotonically noncompact cell class. *F–J*: pyramidal-to-basket-cell connection. *F*: in the averaged voltage trace the EPSPs are seen to consist of a fast rise with a 2-component decay of 6.8 and 60 ms. *G*: voltage-clamp current. *H*: deconvolution using the shorter decay time of 6.8 ms. *I*: relative amplitudes showing excellent agreement between these 2 methods for this compact cell. *J*: detail of the pulses. The initial component of the pulse waveforms are almost identical for the current and deconvolution. However, the longer decay component is much stronger in the deconvolution than the voltage-clamp current, consistent with its mechanism being depolarization activated (i.e., an *N*-methyl-D-aspartate component to the synapse or activation of a voltage-gated current).

amplitudes, there are a number of important differences. The voltage-clamp current has the advantage of being less corrupted by noise because the trace is not differentiated, and also gives an indication (depending on the quality of the space clamp) of the current flowing through the synapse. The deconvolved waveform has the advantage of being sharper, particularly for electronically extended neurons and, importantly, it is measured in current-clamp mode in which the neuron is in its natural state. This allows for the measurement of the normal activation of voltage-gated processes, such as the removal of the magnesium block of the NMDA channels, that are suppressed in voltage-clamp mode. In many studies of ongoing activity, in slices or in vivo, current-clamp mode is preferable due to a desire not to disrupt the firing pattern of the neuron being measured. For such cases, the voltage-deconvolution method described here provides a useful tool for the acquisition of data with high temporal detail.

APPENDIX

Cable theory analysis of voltage deconvolution

The effect of dendritic filtering on voltage-clamp current and voltage deconvolution measurements will be illustrated through the analysis of a simple cable model neuron with two dendrites. This two-dendrite extension of the Rall model (Rall 1969, 1977) is necessary since a soma with a single dendrite misses the current lost from the soma to other dendrites. To ease the notation and to keep the analysis general, time will be measured in units of the passive time constant τ, voltage will be measured from its resting value $v = V - E_m$, and distance along the dendrite x (with $x = 0$ at the soma) will be measured in units of the space constant λ. The voltage in a dendrite obeys

$$\frac{\partial v}{\partial t} = -v + \frac{\partial^2 v}{\partial x^2} + \delta(x - y)\alpha(t) \qquad (A1)$$

where it is assumed that there is a current injection with waveform $\alpha(t)$ at a position $x = y$ (in dendrite a only). A synapse is of course better modeled as a conductance change. However, it is considered that the conductance is sufficiently small such that the voltage dependence of the synaptic drive can be safely neglected (Richardson and Gerstner 2005b). This was shown to be a good approximation in the experiment for EPSPs in Fig. 7.

The soma is modeled as an isopotential compartment of area A_s, with the same passive membrane properties as the dendrites

$$\frac{dv_s}{dt} = -v_s + \rho \frac{\partial v_a}{\partial x_a}\bigg|_{x_a=0} + \rho \frac{\partial v_b}{\partial x_b}\bigg|_{x_b=0} \qquad (A2)$$

where the ratio $\rho = A_d/A_s$ (where A_d is the surface area of a space constant's worth of dendrite) measures the relative effective sizes of the dendritic and somatic compartments.

The dynamics of the system are therefore governed by three equations: two of the *Eq.* A*1* type, for each dendrite v_a, v_b (with no

synapse on dendrite a and one synapse on dendrite b); and one of the *Eq.* A2 type for the somatic voltage (see Fig. 6*A*). These are supplemented by the matching condition that at $x_{a,b} = 0$, then $v_a = v_b = v_s$.

DECONVOLUTION. *Equation* A2 shows that the somatic voltage deconvolution is proportional to the net current flowing into the soma

$$D(t) = \rho \left.\frac{\partial v_a}{\partial x_a}\right|_{x_a=0} + \rho \left.\frac{\partial v_b}{\partial x_b}\right|_{x_b=0} \tag{A3}$$

which for the two-dendrite case here is equivalent to the difference between the magnitudes of current flowing into the soma from the activated dendrite b and out of the soma to the inactivated dendrite a.

VOLTAGE-CLAMP CURRENT. In voltage-clamp mode the somatic voltage is kept fixed at rest, $v_s = 0$, by the injection of a current

$$I_{vc} = -\frac{1}{R_d}\left.\frac{\partial v_b}{\partial x_b}\right|_{x_b=0}^{v_s=0} \tag{A4}$$

where R_d is the membrane resistance of one space-constant's worth of dendrite and where it should be noted that the voltage-clamp current is independent of the somatic area.

Two limits will now be considered: that of large somata for which $\rho \to 0$ and small somata for which $\rho \to \infty$.

A LARGE SOMA. In this case the voltage solutions for the deconvolved voltage can be expanded perturbatively as a series in the small quantity $\rho = A_d/A_s$. For example, the somatic voltage is written

$$v_s = v_{s0} + \rho v_{s1} + \rho^2 v_{s2} + \cdots \tag{A5}$$

At zero order in ρ, *Eq.* A2 gives immediately that $v_{s0} = 0$. Electrophysiologically, this means that the soma is sufficiently large that it is not significantly depolarized by any current flowing from the dendrites. Because of this, no current flows from the soma to dendrite a and so $v_{a0} = 0$. To the next order in the approximation, it is seen that *Eq.* A2 can be written

$$\frac{\partial v_{s1}}{\partial t} + v_{s1} = \left.\frac{\partial v_{b0}}{\partial x_b}\right|_{x_b=0} = \left.\frac{\partial v_b}{\partial x_b}\right|_{x_b=0}^{v_s=0} \tag{A6}$$

The left-hand side of this equation is the deconvolved somatic voltage and the central term is the current flowing into the soma. However, because to zero order the somatic voltage remains constant, this current is equivalent to that flowing into the soma if it were clamped at $v = 0$ (the term on the right-hand side of *Eq.* A6). This current is the inverse of the balance current that would be injected in a voltage-clamp experiment, so it is seen that in the limit of a large somata the deconvolved voltage is directly proportional to the current recorded in current clamp.

A SMALL SOMA. In this limit, $\rho = A_d/A_s \to \infty$, the somatic *Eq.* A2 reduces to a gradient matching between the two dendrites. Physiologically, the somatic conductance and capacitance are so small that the current passes from dendrite b directly into dendrite a without attenuation. Thus the problem reduces to a single dendrite, for which the voltage is measured at $v = 0$ (the putative soma), with a current injection at y described by *Eq.* A1. Clearly, this model is also applicable to voltage deconvolution on a long dendrite.

General mathematical solution. It will be useful in the following to calculate the response to an instantaneous charge injection, equivalent to replacing $\alpha(t)$ with the Dirac delta function $\delta(t)$ in *Eq.* A1. The solution of this equation on an infinite cable

$$\mathcal{G}_0(x, t) = \Theta(t)\,\frac{e^{-t}}{\sqrt{4\pi t}}\,e^{-x^2/4t} \tag{A7}$$

can be used to construct the solutions on the finite cable of length $2L$. In terms of this quantity, the deconvolution can be written as

$$\sum_{k=-\infty}^{\infty}\left[\frac{(y+2kL)^2}{4t^2} - \frac{1}{2t}\right]\mathcal{G}_0\,(y+2kL,\,t) = f_D \tag{A8}$$

whereas the current flowing into the soma in voltage-clamp can be written

$$\left.\frac{\partial \mathcal{G}_{vc}}{\partial x}\right|_{x=0}^{v=0} = \sum_{k=-\infty}^{\infty}(-1)^k\,\frac{(y+2kL)}{t}\,\mathcal{G}_0\,(y+2kL,\,t) = f_{vc} \tag{A9}$$

The notations f_D, f_{vc} have been used because these quantities are the deconvolution and voltage-clamp dendritic filters of the current waveform $\alpha(t)$ injected at y. Both these filters are functions of the synapse location. Thus

$$D(t) = \int_0^t ds\,\alpha(t-s) f_D(s) \tag{A10}$$

$$I_{vc} = -\frac{1}{R_d}\int_0^t ds\,\alpha(t-s) f_{vc}(s) \tag{A11}$$

These filters will now be examined for the cases of proximal and distal synapses.

Proximal synapses. A synapse at $y \ll L$ is considered. The filters (*Eqs.* A8 and A9) can be expanded, the first-order terms can be kept to give a reasonable approximation for $t \ll 1$, $t \ll L^2$

$$f_D(t) \simeq \left(\frac{y^2}{4t^2} - \frac{1}{2t}\right)\frac{e^{-y^2/4t}}{\sqrt{4\pi t}} \tag{A12}$$

$$f_{vc}(t) \simeq \frac{y}{t}\,\frac{e^{-y^2/4t}}{\sqrt{4\pi t}} \tag{A13}$$

The deconvolution filter f_D peaks at $t \simeq 0.09y^2$, decays from this peak as $t^{-5/2}\exp(-y^2/4t)$, changes sign at $t \simeq y^2/2$ (at this point the rate at which the current is lost through dissipation along the dendrite becomes greater than the rate the soma charges up—this effect would also be seen in a single dendrite), and reaches a minimum at $t \simeq 0.91y^2$. The voltage-clamp filter f_{vc} peaks at $t \simeq 0.17y^2$ and decays from this peak as $t^{-3/2}\exp(-y^2/4t)$: it does not change sign because the current flows only into the soma. Thus the deconvolution filter peaks earlier and is sharper than the voltage-clamp filter—it gives a sharper picture of the synaptic current $\alpha(t)$.

Distal synapses. A distal synapse at $y = L$ is now considered. The filters (*Eqs.* A8 and A9) are best considered in their Fourier series representations. To leading order in the late time expansion, it is seen that

$$f_D(t) \simeq \frac{1}{L}\left(\frac{\pi}{L}\right)^2 \exp\left\{-t\left[1 + \left(\frac{\pi}{L}\right)^2\right]\right\} \tag{A14}$$

$$f_{vc}(t) \simeq \frac{1}{L}\left(\frac{\pi}{L}\right) \exp\left\{-t\left[1 + \left(\frac{\pi}{2L}\right)^2\right]\right\} \tag{A15}$$

It should be noted that for distal synapses f_D is positive at late times. Furthermore, the time constant for the filter is shorter for f_D than for f_{vc}; thus the voltage deconvolution waveform is again sharper than the voltage-clamp current. This effect can be significant: for $L = 0.5\lambda$ the deconvolution filter decays with a time constant of about $\tau/40$, whereas for voltage clamp it is approximately $\tau/10$.

It should be noted that these arguments may not hold unqualified for more detailed membrane models that include voltage-gated currents, or that treat the effect of nonhomogeneous channel densities (London et al. 1999; Stuart and Spruston 1998). For such detailed models the precise relation between voltage clamp and deconvolution remains a topic for further analysis.

ACKNOWLEDGMENTS

We thank W. Gerstner and H. Markram for useful discussions and support.

GRANTS

This work was supported by a Human Frontiers Science Program Organization grant to G. Silberberg and M.J.E. Richardson holds a Research Councils United Kingdom Academic Fellowship.

REFERENCES

Abbott LF, Varela JA, Sen K, Nelson SB. Synaptic depression and cortical gain control. *Science* 275: 220–224, 1997.

Agmon-Snir H, Segev I. Signal delay and input synchronization in passive dendritic structures. *J Neurophysiol* 70: 2066–2085, 1993.

Ahmed B, Anderson JC, Douglas RJ, Martin KAC, Whitteridge D. Estimates of the net excitatory currents evoked by visual stimulation of identified neurons in the cat visual cortex. *Cereb Cortex* 8: 462–476, 1998.

Banitt Y, Martin KAC, Segev I. Depressed responses of facilitatory synapses. *J Neurophysiol* 94: 865–870, 2005.

Brunel N, Hakim V, **Richardson MJE.** Firing-rate resonance in a generalized integrate-and-fire neuron with subthreshold resonance. *Phys Rev E Stat Nonlin Soft Matter Phys* 67: 051916, 2003.

Chadderton P, Margrie TW, Häusser M. Integration of quanta in cerebellar granule cells during sensory processing. *Nature* 428: 856–860, 2004.

Cox SJ. Estimating the location and time course of synaptic input from multi-site potential recordings. *J Comput Neurosci* 17: 225–243, 2004.

Cox SJ, Griffith BE. Recovering quasi-active properties of dendrites from dual potential recordings. *J Comput Neurosci* 11: 95–110, 2001.

Dempster J. The use of the driving function in the analysis of endplate current kinetics. *J Neurosci Methods* 18: 277–285, 1986.

Dityatev AE, Altinbaev RS, Astrelin AV, Voronin LL. Combining principal component and spectral analyses with the method of moments in studies of quantal transmission. *J Neurosci Methods* 130: 173–199, 2003.

Fuhrmann G, Markram H, Tsodyks M. Spike frequency adaptation and neocortical rhythms. *J Neurophysiol* 88: 761–770, 2002.

Häusser M, Roth A. Estimating the time course of the excitatory synaptic conductance in neocortical pyramidal cells using a novel voltage jump method. *J Neurosci* 17: 7606–7625, 1997.

Hinrichs H, Scholz M, Tempelmann C, Woldorff MG, Dale AM, Heinze HJ. Deconvolution of event-related fMRI responses in fast-rate experimental designs: tracking amplitude variations. *J Cogn Neurosci* 12: 76–89, 2000.

Hodgkin AL, Huxley AF. A quantitative description of membrane current and its application to conductance and excitation in nerve. *J Physiol* 117: 500–544, 1952.

Jack JJB, Redman SJ, Wong K. The components of synaptic potentials evoked in cat spinal motoneurones by impulses in single group Ia afferents. *J Physiol* 321: 65–96, 1981.

Kleppe IC, Robinson HPC. Determining the activation time course of synaptic AMPA receptors from openings of colocalized NMDA receptors. *Biophys J* 77: 1418–1427, 1999.

Koch C. Cable theory in neurons with active linearized membrane. *Biol Cybern* 50: 15–33, 1984.

Koch C, Segev I. *Methods in Neuronal Modeling: From Ions to Networks* (2nd ed.). Cambridge, MA: MIT Press, 1998.

London M, Meunier C, Segev I. Signal transfer in passive dendrites with nonuniform membrane conductance. *J Neurosci* 19: 8219–8233, 1999.

Mauro A, Conti F, Dodge F, Schor R. Subthreshold behavior and phenomenological impedance of the squid giant axon. *J Gen Physiol* 55: 497–523, 1970.

Neher E, Sakaba T. Combining deconvolution and noise analysis for the estimation of transmitter release rates at the calyx of Held. *J Neurosci* 21: 444–461, 2001.

Neher E, Sakaba T. Combining deconvolution and fluctuations analysis to determine quantal parameters and release rates. *J Neurosci Methods* 130: 143–157, 2003.

Rall W. Distinguishing theoretical synaptic potentials computed for different soma-dendritic distributions of synaptic input. *J Neurophysiol* 30: 1138–1168, 1967.

Rall W. Time constants and electrotonic length of membrane cylinders and neurons. *Biophys J* 9: 1483–1508, 1969.

Rall W. Core conductor theory and cable properties of neurons. In: *Handbook of Physiology. The Nervous System. Cellular Biology of Neurons*. Bethesda, MD: Am. Physiol. Soc., 1977, sect. 1, vol. I, pt. 1, p. 39–98.

Richardson MJE, Brunel N, Hakim V. From subthreshold to firing-rate resonance. *J Neurophysiol* 89: 2538–2554, 2003.

Richardson MJE, Gerstner W. Synaptic shot noise and conductance fluctuations affect the membrane voltage with equal significance. *Neural Comput* 17: 923–947, 2005b.

Richardson MJE, Melamed O, Silberberg G, Gerstner W, Markram H. Short-term synaptic plasticity orchestrates the response of pyramidal cells and interneurons to population bursts. *J Comput Neurosci* 18: 323–331, 2005a.

Rinzel J, Ermentrout GB. Analysis of neural excitability and oscillations. In: *Methods in Neuronal Modeling. From Synapses to Networks*, edited by Koch C, Segev I. Cambridge, MA: MIT Press, 1989, p. 135–169.

Roth A, Häusser M. Compartmental models of rat cerebellar Purkinje cells based on simultaneous somatic and dendritic patch-clamp recordings. *J Physiol* 535: 445–472, 2001.

Silberberg G, Markram H. Disynaptic inhibition between neocortical pyramidal cells mediated by Martinotti cells. *Neuron* 53: 735–746, 2007.

Silberberg G, Wu CZ, Markram H. Synaptic dynamics control the timing of neuronal excitation in the activated neocortical microcircuit. *J Physiol* 556: 19–27, 2004.

Stuart G, Spruston N. Determinants of voltage attenuation in neocortical pyramidal neuron dendrites. *J Neurosci* 18: 3501–3510, 1998.

Surkis A, Peskin CS, Tranchina D, Leonard CS. Recovery of cable properties through active and passive modeling of subthreshold membrane responses from laterodorsal tegmental neurons. *J Neurophysiol* 80: 2593–2607, 1998.

Thomson AM, Deuchars J. Temporal and spatial properties of local circuits in neocortex. *Trends Neurosci* 17: 119–126, 1994.

Tsodyks MV, Markram H. The neural code between neocortical pyramidal neurons depends on neurotransmitter release probability. *Proc Natl Acad Sci USA* 94: 719–723, 1997.

Tuckwell HC. *Introduction to Theoretical Neurobiology: Linear Cable Theory and Dendritic Structure* (Cambridge Studies in Mathematical Biology). Cambridge, UK: Cambridge Univ. Press, vol. 1, 1988.

Wong K, Redman S. The recovery of a random variable from a noisy record with application to the study of fluctuations in synaptic potentials. *J Neurosci Methods* 2: 389–409, 1980.